3-Dimensional stress analysis of O-ring under uniform squeeze rate and internal pressure by photoelastic experimental hybrid method[†]

J. H. Nam[1], J. S. Hawong[1,*], Y. Liu[2] and D. C. Shin[3]

[1]*School of Mechanical Engineering, Yeungnam University, Dae-dong, Gyeongsan, Gyeongbuk 712-749, Korea*
[2]*Graduate School of Mechanical Engineering, Yeungnam University, Dae-dong, Gyeongsan, Gyeongbuk, 712-749 Korea*
[3]*School of Mechanical Engineering, Pusan National University, 30, Jangjeon, Geumjeong, Busan 609-735, Korea*

Abstract

Until now, studies have shown that stresses on the plane (y-z plane) perpendicular to the circumferential direction (x-axis) of an O-ring do exist. Stresses on the planes (x-y plane and x-z plane) parallel to the circumferential direction of the O-ring have not been reported to exist. In this study however, it is demonstrated through a 3-dimensional stress analysis that stresses on the x-y plane and x-z plane of the O-ring under uniform squeeze rate and internal pressure do exist. Therefore, to study effectively 3-dimensional stress distributions of an O-ring under these loadings, stress distributions of every plane should be analyzed. This study develops a photoelastic experimental hybrid method to analyze 3-dimensional stress distributions of an O-ring under uniform squeeze rate and internal pressure, and uses it to determine the stress distributions in every plane, including the Von Mises equivalent stresses, at any arbitrary point of the O-ring under uniform squeeze rate and internal pressure.

Keywords: O-ring; Uniform squeeze; Stress analysis, Photoelastic experimental hybrid method; Von Mises equivalent stress

---

1. Introduction

Machine elements are usually interconnected and are in constant contact with other elements during operation. This causes stress concentrations to be produced at their contact points. Stress concentrations can greatly affect the life and function of a machine; hence, it is important that the stresses at the contact points are analyzed. In the past decades, considerable attention has been paid to finding stress solutions for elastic contact problems.[1-2]

The rubber O-ring is one of the important machine parts widely used as the packing element for high pressure vessels, airplane parts, atomic plant and rocket parts, etc. When metal elements and O-rings are assembled, the O-rings are generally under uniform squeeze rates and internal pressures. The stresses developed in an O-ring as a result of uniform squeeze and internal pressures can have a great impact on the operative life as well as reliability of the O-ring. To design optimum O-rings that will ensure good packing condition and safety without failure, the stresses of the O-rings under uniform squeeze rates and internal pressures should be analyzed.

Until now, only cross-sectional stresses of the O-ring have been analyzed. [3-5] Recently, the cross sectional stresses of an X-ring were analyzed using finite element analysis [6]. The 3-dimensional stresses have not been analyzed. Therefore, this study aims to analyze the 3-dimensional stresses of an O-ring under uniform squeeze rate and internal pressures using the stress freezing method and 3-dimensional photoelastic experiment. The objectives of this paper are as follows: (i) development of the photoelastic experimental hybrid method for 3-dimensional stress analysis of the O-ring, (ii) application of the photoelastic experimental hybrid method for 3-dimensional stress analysis of the O-ring to the 3-dimensional stress analysis of the O-ring, (iii) contact stress analysis and internal stress analysis of the O-ring in the y-z plane, x-y plane and x-z plane, and (iv) 3-dimensional stress analysis and estimation of the Von Mises equivalent stresses of arbitrary internal points of the O-ring.

2. Basic theory

2.1 Hertz contact theory

Eq. (1) gives the stress components of plane stresses using potential functions ϕ and ψ of Muskhelishvili [7].

$$
\begin{aligned}
\sigma_x &= \mathrm{Re}\left[2\phi(z) - \bar{z}\phi'(z) - \psi(z) \right] \\
\sigma_y &= \mathrm{Re}\left[2\phi(z) + \bar{z}\phi'(z) + \psi(z) \right] \\
\tau_{xy} &= \mathrm{Im}\left[\bar{z}\phi'(z) + \psi(z) \right]
\end{aligned}
\tag{1}
$$

Contact problems are generally considered half plane problems. If the upper portion of a body (z>0) is half plane, complex functions ϕ and ψ are involved in the region. Therefore, the analytic complex function in the half plane of the lower portion of the body (z<0) is defined by Eq. (2a) [8].

$$\phi(\overline{z}) = -\overline{\phi(z)} - \overline{z}\,\overline{\phi'(z)} - \overline{\Psi(z)} \tag{2a}$$

$$\Psi(z) = -\phi(z) - \overline{\phi(\overline{z})} - z\phi'(z) \tag{2b}$$

Since stress functions are analytic functions, they can be represented as power series as shown in Eq. (3):

$$\phi(z) = \sum_{n=0}^{N} C_n z^{\frac{n}{2}}, \quad \Psi(z) = \sum_{n=0}^{N} D_n z^{\frac{n}{2}}. \tag{3}$$

Substituting Eq. (3) into Eq. (2b), the equation showing the relation between the complex coefficients of a complex function is obtained and is shown in Eq. (4):

$$D_n = -\frac{n}{2}C_n - \overline{C}_n. \tag{4}$$

Substituting Eq. (4) into Eq. (3) and the resulting expression in (1), Eq. (5) is obtained.

$$\sigma_x(z) = \sum_{n=1}^{N} \text{Re}\left\{ C_n\left[2F(n,z) - G(n,z)\right] + \overline{C}_n F(n,z) \right\}$$

$$\sigma_y(z) = \sum_{n=1}^{N} \text{Re}\left\{ C_n\left[2F(n,z) + G(n,z)\right] - \overline{C}_n F(n,z) \right\} \tag{5}$$

$$\tau_{xy}(z) = \sum_{n=1}^{N} \text{Im}\left\{ C_n G(n,z) - \overline{C}_n F(n,z) \right\}$$

where $F(n,z) = \frac{n}{2}z^{\frac{n}{2}-1}$, $G(n,z) = \frac{n}{2}\left[\left(\frac{n}{2}-1\right)\overline{z} - \frac{n}{2}z\right]z^{\frac{n}{2}-2}$.

2.2 Photoelastic experimental hybrid method

Eq. (6a) describes the stress optic law for an isotropic material [9].

$$\left(\frac{f_\sigma \cdot N_f}{t}\right)^2 = \left(\sigma_x - \sigma_y\right)^2 + \left(2\tau_{xy}\right)^2 \tag{6a}$$

$$\left(\frac{f_\sigma \cdot N_f}{t}\right)^2 - \left(\sigma_x - \sigma_y\right)^2 - \left(2\tau_{xy}\right)^2 = D(\varepsilon) \tag{6b}$$

where f_σ is the stress fringe value, N_f is the fringe order, and t is the thickness of specimen.

After precise experimental data are substituted into Eq. (6a), errors are produced as shown in Eq. (6b); therefore D(ε) cannot be zero. In order to minimize the errors, Hook-Jeeves numerical method is used in this research [10] with the approaching conditions being D(ε) ≤ 10^{-5}. Substitution of Eq. (5)

in Eq. (6b) gives Eq. (7).

$$D(\varepsilon) = \left(\frac{f_\sigma \cdot N_f}{t}\right)^2$$
$$-\left\{\sum_{n=1}^{N} a_n \text{Re}\left[2F(n,z) - 2G(n,z)\right] + \sum_{n=1}^{N} b_n \text{Im}\left[2F(n,z) + 2G(n,z)\right]\right\}^2$$
$$-\left\{\sum_{n=1}^{N} a_n \text{Im}\left[2G(n,z) - 2F(n,z)\right] + \sum_{n=1}^{N} b_n \text{Re}\left[2F(n,z) + 2G(n,z)\right]\right\}^2 \tag{7}$$

If the measured fringe orders (N_f), the position coordinates of the measured fringe orders (z = x +iy), the thickness of the specimen (t) and the stress fringe value (f_σ) are substituted in Eq. (7), then Eq. (7) becomes a function of a_n and b_n only. By applying the Hook-Jeeves numerical method to Eq. (7) with experimental data, a_n and b_n are determined when the limit of errors is satisfied. A substitution of the determined values of a_n and b_n into the corresponding equation gives the stress functions $\phi(z)$ and $\psi(z)$. Putting the values of $\phi(z)$ and $\psi(z)$ into Eq. (1) allows the stress components σ_x, σ_y and τ_{xy} produced in the structure under an arbitrary load to be determined. This procedure is called the photoelastic experimental hybrid method.

3. Experiment and experimental method

3.1 Specimen and experimental method

3.1.1 Slicing method

Epoxy resin prepared from Araldite (CY 230) and hardener (HY 956) in a weight ratio of 10:2 was used in this research. Fig. 1(a) shows the O-ring specimen molded from the epoxy resin, and Fig. 1(b) shows the coordinates and planes (x-z, y-z and x-y) of the O-ring. The x-axis is along the circumferential direction of the O-ring.

Fig. 1(c) shows positions from which slices were cut and principal stresses measured. The numbers (1, 2,…,9) are the planes from which the slices were cut while the capital alphabets (A, B, …, O) are the points at which the principal stresses are calculated.

Slice 1 is in the y-z plane, slices 2, 8 and 9 are in the x-y plane while slices 3, 4, 5, 6 and 7 are in the x-z plane. Every slice was cut from slice 1 as the reference. The centers of slices 2 and 3 are identical to the center of the O-ring. Slices 4 and 7 were cut from a distance of about 0.5 mm outward from both ends of the contact surface of the lower side. On the other hand, slices 5 and 6 were cut from a distance of about 0.5 mm inward from both ends of the contact surface of the lower side while slices 8 and 9 were cut from a distance of about 1 mm inward from both the upper and lower contact surfaces. The cross sectional diameter of the O-ring from which slices were obtained was 6.98 ± 0.15 mm with an inner diameter of 121.5 ± 0.94 mm. The stress fringe value and elastic modulus of epoxy resin used in this study were found to be 46.6 mm/kg (0.457 m/N) and 1.62 kg/mm^2 (15.88 MPa), respectively, at
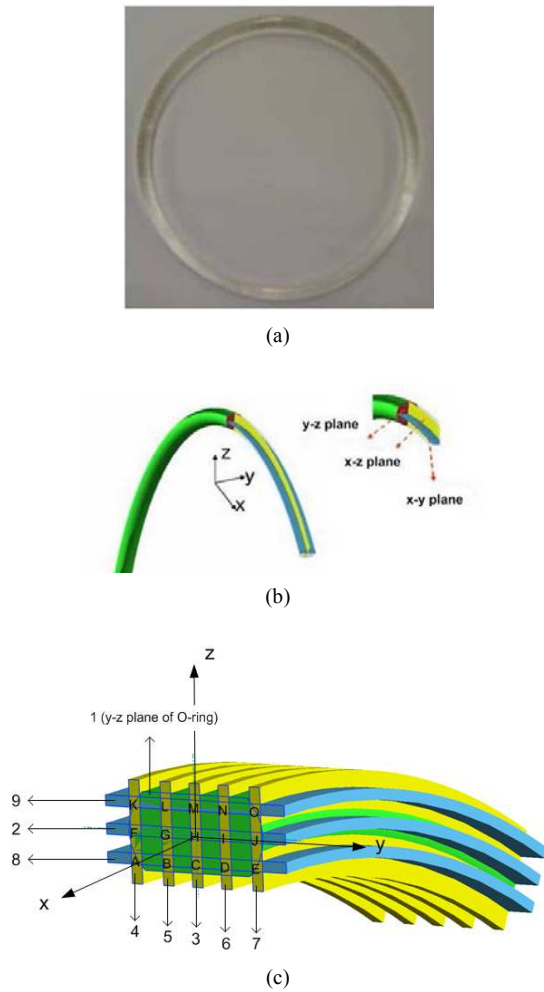
(a)

(b)

(c)

Fig. 1. (a) Specimen of molded O-ring; (b) Coordinates and planes of O-ring; (c) Positions from where slices were cut and principal stress are measured.

Fig. 2. Flow chart of photoelastic experimental hybrid method for 3-dimensional stress analysis.

(a) y-z plane

(b) x-y plane and x-z plane
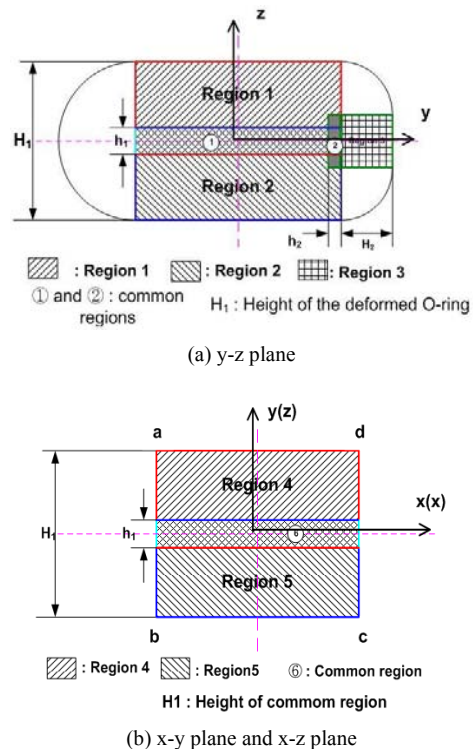
Fig. 3. Stress analysis regions for 3-dimensional photoelastic experiment.

55°C (i.e. stress freezing temperature). To obtain samples for analysis, slices with a thickness of about 1 mm were cut using the detail saw and finished using sand paper. The finished slices were put into a box containing a mixed solution of α-Bromnaphtalene and fluid paraffin at a volume ratio of α-Bromnaphtalene: fluid paraffin = 1: 0.585. The glass box with finished slices was put on the loading position of the transparent experimental device and isochromatic fringe patterns captured and recorded using a digital camera.

Using the loading device developed by the authors [11], uniform squeeze rates and internal pressures were applied to the O-ring made from epoxy resin. Fig. 2 shows the flow chart detailing the procedure of the photoelastic experimental hybrid method used in this research.

3.2 Stress analysis regions

In 3-dimensional stress analysis of the O-ring, each plane of the O-ring is divided into several regions. Fig. 3 shows the various regions into which the O-ring was divided and from
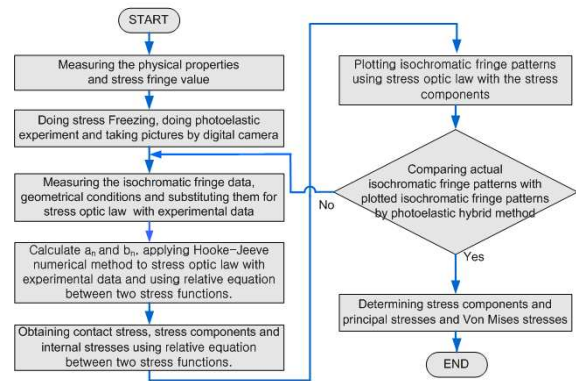
which experimental data for 3-dimensional photoelastic experiment were measured. y-z plane is divided into region 1, region 2 and region 3. Experimental data measured from region 1, region 2 and region 3 was respectively used to analyze the stresses of region 1, region 2 and region 3. x-y plane and x-z plane was divided into region 4 and region 5, and experimental data obtained from region 4 and region 5 was applied to analyze the stresses of regions 4 and 5, respectively.

The a-b face of x-y plane (a-b included the y-face) is the face where internal pressure was applied. The c-d face of x-y plane (c-d included y-face) is the front surface. The a-d face of the x-z plane (a-d included z-face) and b-c face of the x-z

plane (b-c included z-face) are, respectively, the contact faces of the upper side and lower side.

4. Experimental results and discussion

Fig. 4 shows the actual isochromatic fringe pattern of three slices cut from the stress frozen O-ring shown in Fig. 1(c) when the squeeze rate is 20% and internal pressure 7.84 MPa (80 kg/cm^2). Fig. 4(a) and (c) are the isochromatic fringe patterns of the y-z and x-y planes, respectively, showing the stress distributions of the O-ring under internal pressure and uniform squeeze rate.

On the other hand, Fig. 4(b) shows the isochromatic fringe pattern of the x-z plane showing the stress distributions of the upper and lower contact portions of the O-ring. All fringe

patterns are observed to be concentrated on the contact portions. These facts confirm that experiments conducted in this research are valid.

In this study, the contact stress components and internal stress components of each slice as well as the principal stresses of points A, C, E, H, K, M and O in Fig. 1(c) were calculated. In Table 1 the coordinates of points A~O are shown. It is demonstrated from Table 1 that every x-coordinate is zero and this is because the x-axis is in the circumferential direction of the O-ring and the stress distributions of the y-z plane do not change at arbitrary points of the x-axis.

4.1 Actual isochromatics and graphic isochromatics

In this research, the internal stresses and contact stresses of slice 1, slice 3 and slice 8 were analyzed. Fig. 5 shows the actual isochromatic fringe pattern (left side) and graphic isochromatic fringe patterns (right side) of region 1, region 2 and region 3 of slice 1 of the O-ring which was under a uniform squeeze rate of 20% and internal pressure of 7.84 MPa. It is apparent that contact stresses were produced on these slices.

As shown in Fig. 5, the graphic isochromatic fringe patterns are almost identical to the actual fringe patterns. The experimental data was measured on the centerline of the black and white bands. The "+" marks in the isochromatics show positions from where the experimental data were measured. Location of all the "+" marks on the centerline of the black and white bands indicates that the photoelastic experimental hybrid method for 3-dimensional stress analysis introduced in this research is effective.

Figs. 6 and 7 respectively represent the actual isochromatic

Table 1. Position coordinates of points A~O of O-ring under squeeze rate (20%) and internal pressure (80kg/cm^2: 7.84MPa) circumferential direction of O-ring.

Coordinates (x, y, z) / Position	x (mm)	y (mm)	z (mm)
A(F, K)	0.0(0.0, 0.0)	-2.5(-2.5, -2.5)	-1.5(0.0, 2.1)
B(G, C)	0.0(0.0, 0.0)	-1.5(-1.5, -1.5)	-1.5(0.0, 2.1)
C(H, M)	0.0(0.0, 0.0)	0(0,0)	-1.5(0.0, 2.1)
D(I, N)	0.0(0.0, 0.0)	1.5(1.5, 1.5)	-1.5(0.0, 2.1)
E(J, O)	0.0(0.0, 0.0)	2.5(2.5,2.5)	-1.5(0.0, 2.1)

Coordinates of x: arbitrary point along the circumferential direction of O-ring

(a) Slice 1 (y-z plane) (b) Slice 3 (x-z plane) (c) Slice 8 (x-y plane)
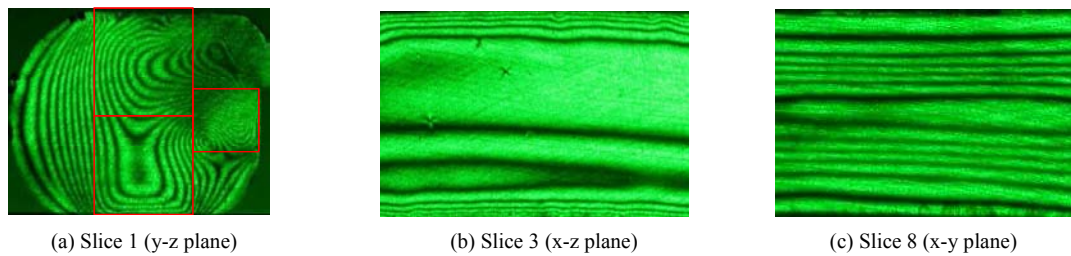
Fig. 4. Isochromatic fringe patterns of each slice of O-ring under uniform squeeze rate (20%) and internal pressure (7.84 MPa).
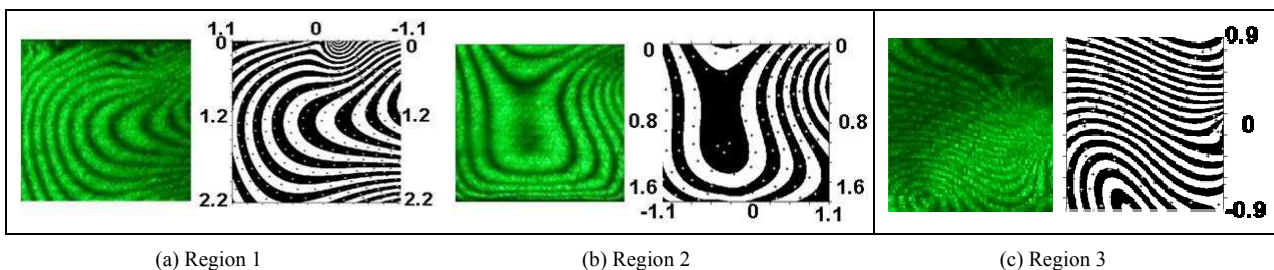

(a) Region 1 (b) Region 2 (c) Region 3

Fig. 5. Actual isochromatic fringe patterns and graphic isochromatic fringe patterns of slice 1 of the O-ring under squeeze rate (20%) and internal pressure (80 kg/cm^2: 7.84 MPa) from the photoelastic experimental hybrid method.

(a) Region 4   (b) Region 5

Fig. 6. Actual isochromatic fringe patterns and graphic isochromatic fringe patterns of slice 3 of the O-ring under squeeze rate (20%) and internal pressure (80 kg/cm^2: 7.84 MPa) from the photoelastic experimental hybrid method.

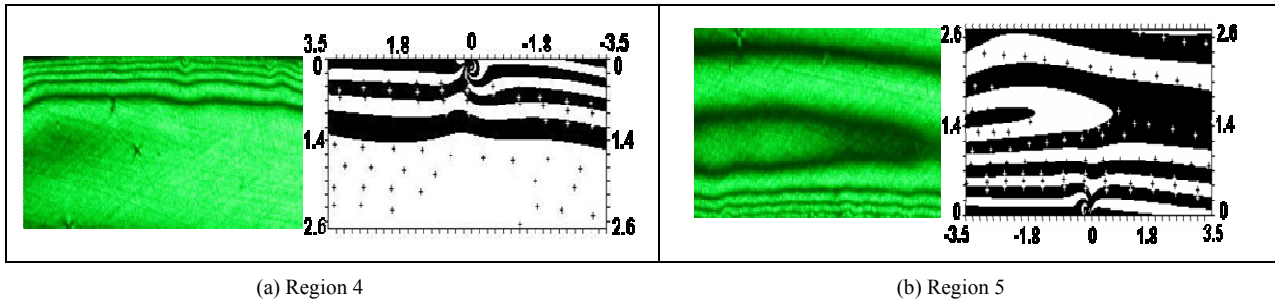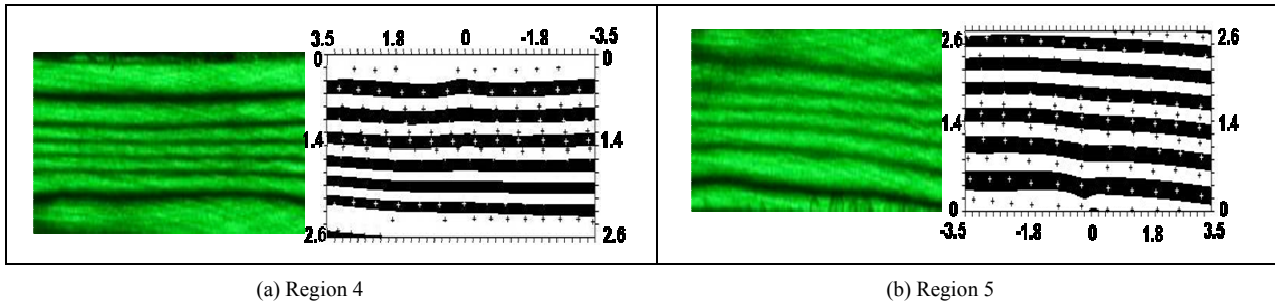(a) Region 4   (b) Region 5

Fig. 7. Actual isochromatic fringe patterns and graphic isochromatic fringe patterns of slice 8 of the O-ring under squeeze rate (20%) and internal pressure (80 kg/cm^2: 7.84 MPa) from the photoelastic experimental hybrid method.

fringe patterns (left side) and graphic isochromatic fringe patterns (right side) in region 4 and region 5 of slice 3 and slice 8 of O-ring under uniform squeeze rate (20%) and internal pressure (9.84 MPa). It is apparent from Figs. 6 and 7 that the graphic isochromatic fringe patterns from the photoelastic experimental hybrid method for 3-dimensional stress analysis are almost identical to the actual isochromatic fringe patterns when the squeeze rate is 20% and internal pressure is 7.84 MPa. Moreover, the location of the "+" marks on the centerline of the black and white bands further confirms the validity of the photoelastic experimental hybrid method introduced in this research for 3-dimensional stress analysis. Figs. 6 and 7 also show that stresses in the x-y and x-z planes do exist..

### 4.2 Contact stresses and internal stresses of y-z plane

4.2.1 Contact stresses of the y-z plane

Fig. 8(a) shows the contact stress distribution of σ_y, σ_z, τ_{yz} on the upper side of the y-z plane of the O-ring under 20% squeeze rate and internal pressure (7.84 MPa) when P_o is 13.94 MPa. The symbols —●—, —■— and —◆— represent the stress components σ_y (σ_y/P_o), σ_z (σ_z/P_o) and τ_{yz} (τ_{yz}/P_o), respectively, for the upper contact side. These experimental results were obtained using the photoelastic experimental hybrid method for 3-dimensional stress analysis developed in this research.

The results indicate that the contact stresses of the upper side of the O-ring were a little bit larger than those on the
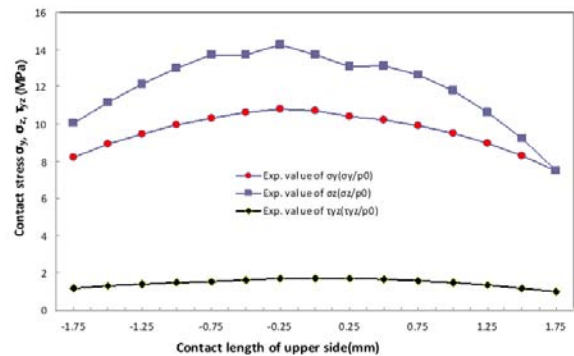
(a) Upper side of y-z plane
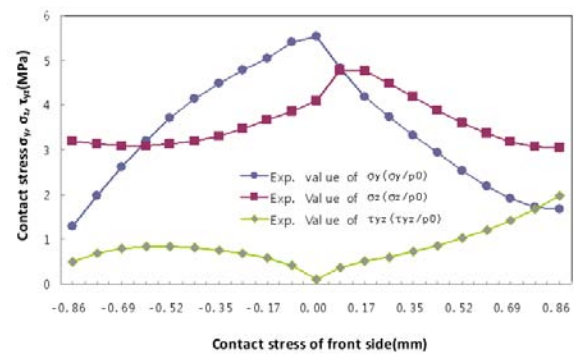
(b) Front side of y-z plane

Fig. 8. Contact stress distribution σ_y, σ_z, τ_{yz} of the upper side for y-z plane (a) and front side y-z plane (b) of the O-ring under squeeze rate (20%) and internal pressure (80 kg/cm^2: 7.84 MPa) with P_o = 13.94 Mpa.

lower side of the O-ring. It is observed from Fig. 8(a), that the maximum of σ_y (σ_y/P_o) is 10.81 (0.775) MPa and it occurred on the left side, at a small distance from the centre of the contact side. The magnitude of σ_y on the left end point of the contact side is almost equal to the magnitude of the internal pressure.

It is also shown from Fig. 8(a), that the maximum of σ_z (σ_z/P_o) is 14.26 (1.023) MPa and is located at the centre of contact side. The value of σ_z on the left end point of the contact side is much larger than the magnitude of the internal pressure. However, at the right end point of the contact side, σ_z is found to be a little bit less than the magnitude of the internal pressure. The maximum of τ_{yz} (τ_{yz}/P_o) is 1.72 (0.123) MPa and it occurs at the centre of the contact side. It is shown from the results of Fig. 8(a) that stress distribution pattern of σ_z (σ_z/P_o) is very similar to that of σ_y (σ_y/P_o); but the magnitudes of σ_z (σ_z/P_o) are larger than those of σ_y (σ_y/P_o). In comparison, it is noted that the stress distribution pattern of τ_{yz} (τ_{yz}/P_o) is different from that of both σ_y(σ_y/P_o) and σ_z(σ_z/P_o). In addition, magnitudes of τ_{yz}(τ_{yz}/P_o) are much less than those of σ_y(σ_y/P_o) and σ_z(σ_z/P_o).

Fig. 8(b) shows contact stress distributions of σ_y, σ_z, τ_{xy} on the front side of the y-z plane of the O-ring under a squeeze rate of 20% and internal pressure of 7.84 MPa. Symbols ━●━, ━■━ and ━◆━ respectively indicate the stress components of σ_y (σ_y/P_o), σ_z (σ_z/P_o) and τ_{xy} (τ_{xy}/P_o) on the front contact side obtained from the photoelastic experimental hybrid method for 3-dimensional stress analysis. As noted from Fig. 8(b), the maximum of σ_y (σ_y/P_o) is 5.53 (0.396) MPa while the maximum of σ_z (σ_z/P_o) is 4.77 (0.342) MPa and both occur at the centre of the contact line. On the other hand, the maximum of τ_{yz}(τ_{yz}/P_o) is 1.97 (0.141) and it occurs at the right end of the contact side. Fig. 8(b) also shows that the distribution patterns and magnitudes of σ_y, σ_z and τ_{yz} are different from each other. Among them, maximum σ_y is the largest and maximum τ_{yz} is the smallest.

4.2.2 Internal stresses of y-z plane

Experimental values of σ_y, σ_z and τ_{xy} in region 1, region 2 and region 3 were obtained from the photoelastic experimental hybrid method developed in this study. For example, Fig. 9 shows the stress contours of (σ_y/P_o) in region 1, region 2 and region 3 of the O-ring under a squeeze rate of 20% and internal pressure of 7.84 MPa, when P_o is 13.94 MPa. It is shown from Fig. 9(a) that even when internal pressure is applied to the O-ring, the stress magnitudes (σ_y/P_o) of region 1 and region 2 are much larger than those of region 3. However, the stress magnitudes (σ_y/P_o) of region 1 are almost equal to those of region 2.

The stress contours of σ_z/P_o in region 1, region 2 and region 3 of the O-ring under 20% squeeze rate and 7.84 MPa internal pressure are shown in Fig. 9(b). It is observed from Fig. 9(b), that the (σ_z/P_o)'s of region 1 and region 2 are much larger than those of region 3. However, the (σ_z/P_o)'s of region 2 are almost equal to those of region 1.
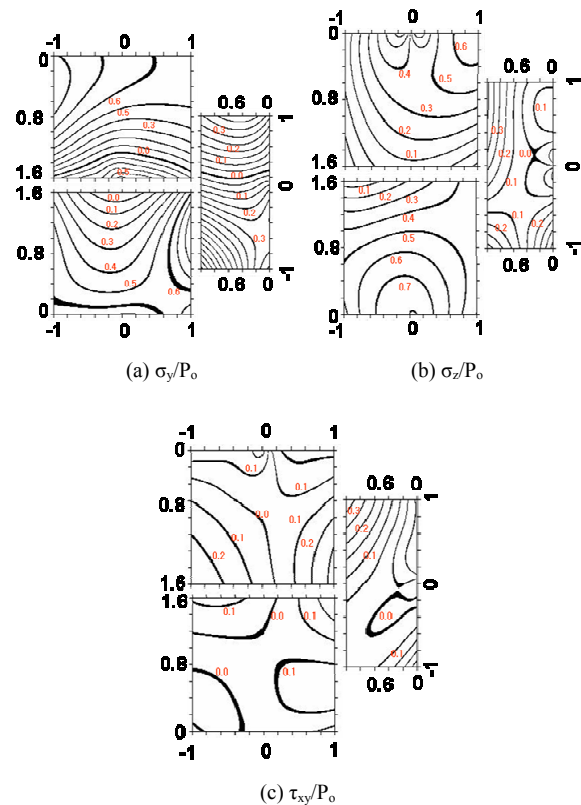

(a) σ_y/P_o

(b) σ_z/P_o

(c) τ_{xy}/P_o

Fig. 9. Stress contours for slice 1 obtained from the hybrid method for the O-ring under squeeze rate (20%) and internal pressure (80kg/cm^2: 7.84MPa) with P_0 = 13.94 Mpa.

Fig. 9(c) represents the stress contours of (τ_{xy}/P_o) in region 1, region 2 and region 3 of O-ring under 20% squeeze rate and 7.84 MPa internal pressure. It is seen from Fig. 9(c) that the (τ_{yz}/P_o)'s in region 3 are larger than (τ_{yz}/P_o)'s in region 1 and region 2. When compared with the magnitudes of (σ_z/P_o) and (σ_y/P_o) of region 1 and region 2, the magnitudes of (τ_{yz}/P_o) in region 1 and region 2 are much smaller. The magnitudes of (τ_{yz}/P_o) in the region 3 were found to be about 40% of those of (σ_y/P_o) or (σ_z/P_o) in region 3.

It is observed from Fig. 9(a) and Fig. 9(b) that the stress distribution patterns of (σ_z/P_o) in region 1 and region 2 are different from those of (σ_y/P_o)'s in region 1 and region 2. It is further noted that while the magnitudes of (σ_z/P_o) in region 1 and region 2 are a little larger than those of (σ_y/P_o) in region 1 and region 2, the magnitudes of (σ_z/P_o) in region 3 are similar to those of (σ_y/P_o) in region 3.

Moreover, the magnitudes of (σ_y/P_o) in region 1 are very similar to those of (σ_y/P_o) in region 2 and the magnitudes of (σ_y/P_o) in region 3 are much less than those of (σ_y/P_o) in region 1 or region 2. The magnitudes of (σ_y/P_o) in region 1 are very similar to those of (σ_z/P_o) in region 2. Stress distribution patterns of (σ_z/P_o) in the region 1 are different from those of (σ_z/P_o) in the region 2. It is also seen that the magnitudes of σ_y/P_o or σ_z/P_o in region 3 are about half of those of region 1 or region 2, respectively. The maximum magnitudes of σ_y/P_o and
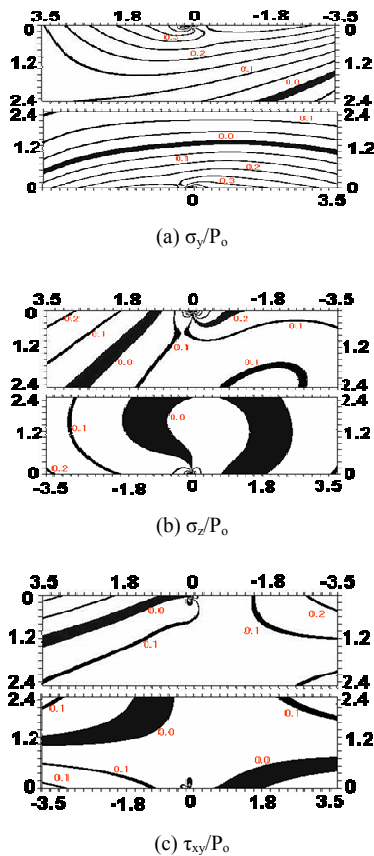
(a) σ_y/P_o

(b) σ_z/P_o

(c) τ_{xy}/P_o

Fig. 10. Stress distributions of slice 3 of the O-ring under squeeze rate (20%) and internal pressure (80kg/cm^2: 7.84MPa).

(a) σ_y/P_o

(b) σ_z/P_o

(c) τ_{xy}/P_o

Fig. 11. Stress distributions of slice 8 of the O-ring under squeeze rate (20%) and internal pressure (80kg/cm^2: 7.84MPa).

σ_z/P_o in region 1 and region 2 are between 6 to 9 times those of τ_{xy}/P_o in region 1 and region 2.

4.2.3 Stress components and principal stresses at a point

The stress components on 3 planes (y-z plane, x-y plane, x-z plane) are needed so as to determine the principal stresses (σ_1, σ_2, σ_3) at any point in a structure under arbitrary loads. In this study, the principal stresses were calculated from the stress components obtained using the developed photoelastic experimental hybrid method for 3-dimensional stress analysis. As noted from Fig. 1(c), the arbitrary points A, B, …, O in arbitrary planes are the points at which the principal stresses are calculated.

In Figs. 10 and 11, the stress contours of σ_x/P_o, σ_z/P_o and τ_{xz}/P_o show how the stresses are distributed in slices 3 and 8 of an O-ring under uniform squeeze rate of 20% and internal pressure of 7.84 MPa. These results were obtained using the developed photoelastic experimental hybrid method for 3-dimensional stress analysis. In slice 3, the maximums of σ_x/P_o, σ_z/P_o and τ_{xz}/P_o occurred on the contact surface of either the upper side or lower side as shown in Fig. 10. The magnitudes of σ_z/P_o and τ_{xz}/P_o were found to be very small compared to the magnitudes of (σ_x/P_o). In slice 8, the magnitudes of σ_y/P_o and τ_{xy}/P_o were almost zero while the magnitudes of σ_x/P_o
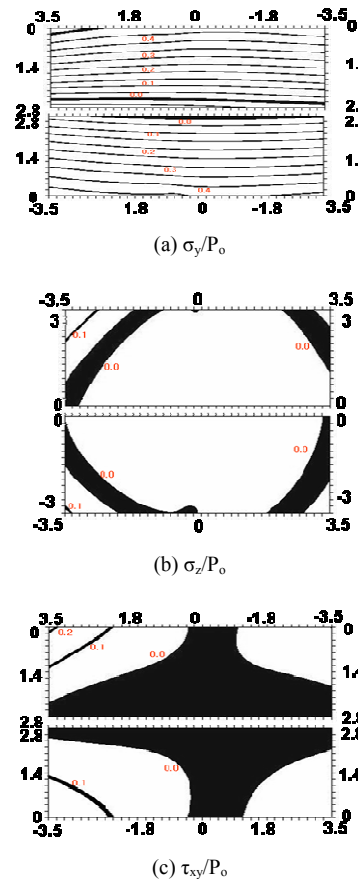
were comparatively high. The stress distributions of the x-z plane (slice 3) are controlled by the squeeze rate while the stress distributions of the x-y planes (slice 8) are controlled by internal pressures.

The above observations suggest that even if internal pressures and squeeze are applied to the O-ring, stresses in the x-axis (i.e., circumferential direction of O-ring) will exist with magnitudes of σ_y and τ_{xy} being small compared with those of σ_x.

Table 2 shows the stress components, principal stresses, maximum shear stresses and Von Mises equivalent stresses at arbitrary points on the O-ring. The Von Mises equivalent stresses were obtained using principal stresses σ_1, σ_2 and σ_3. Experimental values in Table 2 were obtained using the photoelastic experimental hybrid method for 3-dimensional stress analysis.

It is observed from the table that the stress values of each point are almost identical to each other at the same point demonstrating that the photoelastic experimental hybrid method for the 3-dimensional stress analysis developed in this research is valid. However, the values of some principal stresses at the same point are slightly different from each other.

Large principal stresses σ_1 and σ_3 are observed to occur at points C and M which are located at the center of the upper or lower side of the contact surface of the O-ring as shown

Table 2. Stress components of arbitrary point on the 3 planes of the O-ring under squeeze rate and internal pressure: SC-stress components, Pt- point, Pl- plane.

Pt	Pl	σ_i	σ_j	τ_{ij}	σ_{ii}	σ_{jj}	τ_{max}	σ_{eq}
A	y-z	5.54	6.07	0	6.07	5.54	0.31	0.56
	x-z	5.81	6.42	0	6.42	5.81		
	x-y	5.76	5.35	0	5.76	5.35		
C	y-z	10.70	13.70	1.82	14.56	9.84	2.46	3.48
	x-z	10.62	14.07	1.75	14.80	9.89		
	x-y	10.22	10.90	0.16	10.94	10.18		
E	y-z	4.47	0.53	0	4.47	0.53	2.09	2.98
	x-z	4.65	0.64	0	4.65	0.64		
	x-y	4.21	4.82	0	4.82	4.21		
H	y-z	0	0	0	0	0	0	0
	x-z	0	0	0	0	0		
	x-y	0	0	0	0	0		
K	y-z	4.48	0.55	0	4.48	0.55	2.10	2.99
	x-z	4.52	0.65	0	4.52	0.65		
	x-y	4.43	4.85	0	4.85	4.43		
M	y-z	10.72	13.72	1.74	14.52	9.92	2.40	3.40
	x-z	10.37	14.15	1.58	14.72	9.80		
	x-y	10.02	11.21	0.09	11.22	10.01		
O	y-z	5.55	6.08	0	6.08	5.55	0.26	0.57
	x-z	5.99	6.51	0	6.51	5.99		
	x-y	5.11	5.72	0	5.72	5.11		

y-z plane : $\sigma_i = \sigma_y$, $\sigma_j = \sigma_z$, $\tau_{ij} = \tau_{yz}$, $\sigma_{ii} = \sigma_2$, $\sigma_{jj} = \sigma_3$

x-z plane : $\sigma_i = \sigma_x$, $\sigma_j = \sigma_z$, $\tau_{ij} = \tau_{xz}$, $\sigma_{ii} = \sigma_1$, $\sigma_{jj} = \sigma_3$

x-y plane : $\sigma_i = \sigma_x$, $\sigma_j = \sigma_y$, $\tau_{ij} = \tau_{xy}$, $\sigma_{ii} = \sigma_1$, $\sigma_{jj} = \sigma_2$

in Fig. 1(c).

It is also seen from Table 2 that the maximum shear stresses as well as the maximum Von Mises equivalent occurred at points C and M. This means that maximum shear stresses occurred at the point of maximum shear strains. Verification of this concept demonstrates that the experimental results obtained from this study are valid. Based on the results obtained from the analysis of the stress distributions of the O-ring under uniform squeeze rate and internal pressure, the following conclusions are made.

5. Conclusions

(1) The photoelastic experimental hybrid method for 3-dimensional stress analysis has shown that stresses not only exist in the y-z plane as previously reported but also in the x-y plane and x-z plane when O-ring is under uniform squeeze and internal pressure. The processes of determining stresses, principal stresses, maximum shear stress, equivalent stresses, stress distributions, and the graphic isochromatic fringe pattern have been introduced and applied to find the stress components, maximum shear stresses and equivalent stresses of arbitrary points of the O-ring as shown in Table 2.

(2) The maximums of σ_y, σ_z and τ_{xy} on the lower or upper contact surface in the y-z plane of the O-ring occurred at the centre of the contact surface and became smaller as the distance increased from the center of contact surface. The maximum values of τ_{xy} in region 3 of y-z plane occurred at the end point of the right side on the contact surface while the maximum values of σ_x, σ_y, σ_z, τ_{xy}, τ_{xz}, τ_{yz}, σ_1, σ_2, σ_3 as well as maximum equivalent stresses occurred at points C and M whose coordinates are C (3.5, 0, 1.0) and M (3.5, 0, 4.6). The maximum values of σ_x, σ_y and τ_{xy}, on the lower and/or upper contact surface in the x-y plane of the O-ring occurred at the centre of the contact surface and their values reduced as the distance increased from the center of contact surface. While magnitudes of σ_x and σ_z in the x-z plane were small, those of τ_{xz}, were much smaller. These stresses are generally controlled by internal pressures.

(3) The stresses in the y-z plane are controlled by internal pressures and squeeze rates. The stress distribution patterns as well as magnitudes for region 1 and region 2 are generally very similar to each other but the σ_y and σ_z of the lower side (region 2) are a bit larger than those of the upper side (region 1). The σ_y and σ_z of the front side (region 3) were found to be about half of those of the lower side or upper side. Whereas the shear stresses (τ_{yz}) of the lower side are very similar to those of the upper side, it was observed that the shear stresses (τ_{yz}) on the front side are larger than τ_{yz} on the upper side or lower side. In fact the values of τ_{yz} in the front side were found to be 40% of σ_y and σ_z of the front side. In addition, the maximums of σ_y and σ_z in the upper side or lower side are between 6 times and 9 times of the maximum shear stress τ_{yz}.

References

[1] H. D. Conway, The pressure distribution between two elastic bodies in contact, *Z. Angew. Math. Phys.*, 7 (1956) 460-465.

[2] A. Francavilla and O. C. Zienkiewicz, Note on numerical computation of elastic contact problems, *Int. J. Numer. Methods Eng.*, 9 (4) (1975) 913-924.

[3] A. F George, A. Strozzi and J. I. Rich, Stress fields in a compressed unconstrained elastomeric O-ring seal and a comparison of computer predictions with experimental results, *Tribol. Int.*, 20 (1987) 237-247.

[4] A. Karaszkiewicz, Geometry and contact pressure of an O-Ring mounted in a seal groove, *Ind. Eng. Chem. Res.*, 29

(1990) 2134-2137.

[5] I. K. Lee and C. K. Kim, Numerical simulations on the O-ring extrusion in automotive engines, *Journal of Korean Society of Tribologists & Lubrication Engineers*, 15 (4) (1999) 297-303.

[6] H.-S. Lee, Y.-S. Lee, J.-H. Lee, B.-S. Chun, J.-H. Baek and S.-Y. Kim, A study on the contact stress analysis for X-ring, DOI:10.3795/KSME-A.2008.32.9.733.

[7] N. I. Muskhelishvili, *Some basic problems of mathematical theory of elasticity*, 4th Edition, P. Noordhoff Ltd., Groningen, Netherlands (1963).

[8] D. A. Hills, D. Nowell and A. Sackfield, *Mechanics of elastic contact* (1993).

[9] R. C. Sampson, A stress-optic law for photoelastic analysis of orthotropic composites, *Exp. Mech.*, 10 (1970) 210-215.

[10] M. S. Bazaraa and C. M. Shetty, *Nonlinear programming: theory and algorithms*, John Wiley & Sons Inc., (1979).

[11] J.-H. Nam, J.-S. Hawong, K.-H. Kim, Y. Liu, O.-S. Kwon and S.-H. Park, A study on the development of a loading device using a photoelastic stress freezing method for the analysis of O-ring stress, *Journal of Mechanical Science and Technology*, 24 (3) (2010) 693-701.

Jai-Sug Hawong received a B.S. in Mechanical Engineering from Yeungnam University in 1974. Then he received his M.S. and Ph.D from Yeungnam University in Korea in 1976 and from Kanto Gakuin University in Japan in 1990, respectively. Prof. Hawong is currently a professor at the school of Mechanical Engineering at Yeungnam University, in Gyeongsan city, Korea. He served as President of Korea Society Mechanical Engineering in 2010. Prof. Hawong's research interests include static and dynamic fracture mechanics, stress analysis, experimental mechanics for stress analysis and composite material, etc.

Jeong-hwan Nam received a B.S. in Mechanical Engineering from Yeungnam University in 1986. Then he received his M.S. and Ph.D from Yeungnam University in Korea in 1996 and from Saitama Institute of Technology in Japan in 2005, respectively. Dr. Nam is currently a researcher at the school of Mechanical Engineering at Yeungnam University, in Gyeongsan city, Korea. Dr. Nam's research interests include mechanical design, stress analysis and experimental mechanics for stress analysis, etc.